The Journal of Experimental Biology 214, 2390-2397

doi:10.1242/jeb.055020

RESEARCH ARTICLE

Hyperbaric computed tomographic measurement of lung compression in seals and dolphins

Michael John Moore[1,*], Terrence Hammar[1], Julie Arruda[1], Scott Cramer[1], Sophie Dennison[2], Eric Montie[3] and Andreas Fahlman[1]

[1]Woods Hole Oceanographic Institution, Woods Hole, MA 02543, USA, [2]10 Liberty Ship Way #102, Sausalito, CA 94965, USA and [3]College of Marine Science, University of South Florida, St Petersburg, FL 33701, USA

*Author for correspondence (mmoore@whoi.edu)

Accepted 5 April 2011

SUMMARY

Lung compression of vertebrates as they dive poses anatomical and physiological challenges. There has been little direct observation of this. A harbor and a gray seal, a common dolphin and a harbor porpoise were each imaged post mortem under pressure using a radiolucent, fiberglass, water-filled pressure vessel rated to a depth equivalent of 170 m. The vessel was scanned using computed tomography (CT), and supported by a rail and counterweighted carriage magnetically linked to the CT table movement. As pressure increased, total buoyancy of the animals decreased and lung tissue CT attenuation increased, consistent with compression of air within the lower respiratory tract. Three-dimensional reconstructions of the external surface of the porpoise chest showed a marked contraction of the chest wall. Estimation of the volumes of different body compartments in the head and chest showed static values for all compartments except the lung, which showed a pressure-related compression. The depth of estimated lung compression ranged from 58 m in the gray seal with lungs inflated to 50% total lung capacity (TLC) to 133 m in the harbor porpoise with lungs at 100% TLC. These observations provide evidence for the possible behavior of gas within the chest of a live, diving mammal. The estimated depths of full compression of the lungs exceeds previous indirect estimates of the depth at which gas exchange ceases, and concurs with pulmonary shunt measurements. If these results are representative for living animals, they might suggest a potential for decompression sickness in diving mammals.

Key words: experimental hyperbaric lung compression, dolphin, seal, diving physiology.

INTRODUCTION

Decompression sickness (DCS) can result from the phase change of supersaturated tissues during diver ascent. The resultant potential for gas embolus formation, which may or may not be associated with tissue damage, remains a potential problem for human divers using compressed gas. However, breath-hold divers are also not immune from DCS risk. Paulev showed that rapid, repetitive breath holding in human divers results in DCS (Paulev, 1965). The paradox of marine mammals, birds and reptiles diving routinely to substantial depths without apparent acute or chronic symptoms of DCS has aroused the curiosity of many scientists (Costa et al., 2004; Fossette et al., 2010; Hays et al., 2004; Kooyman, 2006; Ridgway and Howard, 1979; Scholander, 1940; Wilson et al., 1992). Anatomical adaptations thought to be important include: lung collapse, the atelectic collapse of alveoli to shunt blood away from gas exchange surfaces; tracheobronchial compliance changes (Bostrom et al., 2008); and blood redistribution into the rete mirabile in cetaceans and blood sinuses in pinnipeds. Behavioral and physiological adaptations could include diving patterns that minimize DCS risk (Hooker et al., 2009; Zimmer and Tyack, 2007), bradycardia (Harrison and Tomlinson, 1960), and vascular perfusion control (Kooyman, 1985). From indirect measurements, lung collapse has been estimated to occur at 30 m for Weddell seals (Falke et al., 1985) and 70 m for bottlenose dolphins (Ridgway and Howard, 1979), while pulmonary shunt measurements have suggested that gas exchange may not cease until a depth of 170 m even in animals diving with a low lung volume (Kooyman and Sinnett, 1982).

Gas bubbles in stranded aquatic mammals have become a focus of attention since a brief report (Jepson et al., 2003) and later papers on atypical mass strandings of beaked whales (Fernandez et al., 2005) and single strandings of odontocetes (Jepson et al., 2005). These data established the pathobiological basis for a hypothesis (Cox et al., 2006) that beaked whales are acutely (Fernandez et al., 2005), and other odontocetes are perhaps chronically (Jepson et al., 2005; Moore and Early, 2004), at risk of DCS.

We recently observed gas bubbles in seals and dolphins that accidentally drowned in fisheries (i.e. bycaught animals) at 34–120 m depth (Moore et al., 2009), and concluded that these cases are evidence of supersaturation during dives that are prolonged through entanglement. Thus, breath-holding marine mammals that are disturbed during diving may risk clinical symptoms of gas bubble formation, as observed in atypical mass strandings of beaked whales (Fernandez et al., 2005).

The mechanics of lung compression are crucial to understanding gas kinetics in this context. It is important to realize that the depth at which a change from positive to negative buoyancy occurs, as described for right whales (Nowacek et al., 2001), is no absolute indicator of the depth of lung collapse. It is simply the point at which the overall lung buoyancy decreases to where it no longer counteracts the negative buoyancy of the rest of the animal. Active swimming *versus* passive gliding with a favorable buoyancy gradient is further

affected by drag (Miller et al., 2004; Watanabe et al., 2006) and lift (Fish, 1996). Therefore, direct imaging is required to actually document the process of lung compression. Few radiographic efforts to study this in breath-holding divers have been undertaken. Kooyman and colleagues used radiographic contrast media to show that seal tracheal diameters decreased 50% during a dive but that the bronchi narrowed less (Kooyman et al., 1970). Chest radiographs were obtained of breath-holding human divers at depths up to 20 m using submerged X-ray equipment (Data et al., 1979), but no findings were published. We therefore developed an experimental hyperbaric chamber interfaced to an X-ray computed tomography (CT) scanner to more fully examine lung compression in seal and dolphin post-mortem specimens. Measurements of total lung volume, and constituent lung tissue and lung gas were compared between different pressures, enabling an estimate of the depth at which the lung is fully compressed.

MATERIALS AND METHODS

Hyperbaric chamber

The chamber was constructed using the Green Thread 250 Piping System (Fiber Glass Systems, Little Rock, AR, USA) and assembled (Fig. 1) by Corrosion Products and Equipment (Albany, NY, USA). It was composed of a fiberglass pipe (291 cm long, 40.6 cm i.d., 43.2 cm o.d.) with each end glued to a fiberglass flange (11 cm thick, 59.7 cm diameter). End caps (7 cm thick, 59.7 cm diameter) were fastened to each flange with 16 steel bolts (28×220 mm) with lock washers through a rubber gasket. The empty chamber weighed 258 kg. It was mounted with the specimen placed within the chamber closest to the scanner gantry (‘a’ in Fig. 1). The end cap, at this end of the chamber, had 6.4 mm threaded (1/4″ NPT) holes at the top and bottom center at the level of the inner diameter of the tube. This allowed a brass nipple and valve to be installed on the outside edge of the cap to enable addition and removal of water through the lower nipple and water and air through the upper nipple. A pressure gauge was attached between the upper nipple and valve allowing an approximate measure of the internal chamber pressure (±15 kPa). A data logger (DST Milli: Star-Oddi, Reykjavik, Iceland) was placed inside the chamber, providing a high resolution (±1 kPa) record of the dive profile at 1 Hz that was downloaded at the end of the experiment. Once loaded with a specimen and filled with water, the system weighed 985 kg and exceeded the design mass capacity (200 kg) of the CT scanner table. It was therefore suspended over the CT scanner table in an aluminum cradle and rail system. The cradle was attached by four removable bolts to a pair of supporting cars (CAR-BB CB TRAV 4500 W/ SHKL supplied by Harken USA, Pewaukee, WI, USA) on each of two rails that ran parallel to the scanner table and enabled approximately half of the chamber’s length to pass through the scanner gantry. Once loaded with a specimen, the chamber was filled with water and pressurized using a GTP-2157-A aircraft fueling hose tester (Gammon Technical Products Inc., Manasquan, NJ, USA) connected to the lower nipple. A 414 kg counterweight of four lead discs (Nuclead Inc., West Bridgewater, MA, USA) in an aluminum basket was suspended on the end of the chamber furthest from the scanner gantry. This placement moved the center of gravity of the chamber to 93 cm from the counter-weighted end. This configuration resulted in a metal-free imaging window of 130 cm in length between the saddle and the flange at the un-weighted, imaging end of the chamber. The chamber was lowered onto the rail system using a hoist of 2000 kg capacity, which was mounted to a ceiling rail. The chamber movement was synchronized with the CT scanner table *via* a computerized linear drive tracking system designed and supplied by Artec Imaging (Cornelius, NC, USA). This tracking system comprised a magnetic actuator rail and sensor attached to the scanner table by a self-adhesive hook and loop tape, a controlling computer, and a 110 V electric motor (NEMA 34 I-Grade servo motor and encoder no. QCI-A34HC2; Quicksilver Controls Inc., Covina, CA, USA).

Specimens (Table 1)

Animals were received under NOAA permit no. 932-1905-00/MA-009526. A gray (*Halichoerus grypus*, Fabricius) and harp (*Pagophilus groenlandicus*, Erxleben) seal (drowned in fishing nets) and a harbor porpoise (*Phocoena phocoena*, Linnaeus) and common dolphin (*Delphinus delphis*, Linnaeus) (found beached and freshly dead) were transported at ambient temperature to the laboratory. Upon arrival, the specimens were stored at 4°C until each experiment began, less than 12 h after arrival at the laboratory. No specimens were frozen. Each animal was intubated using a human endotracheal tube of suitable size (Hudson RCI, Teleflex Medical Inc., Research

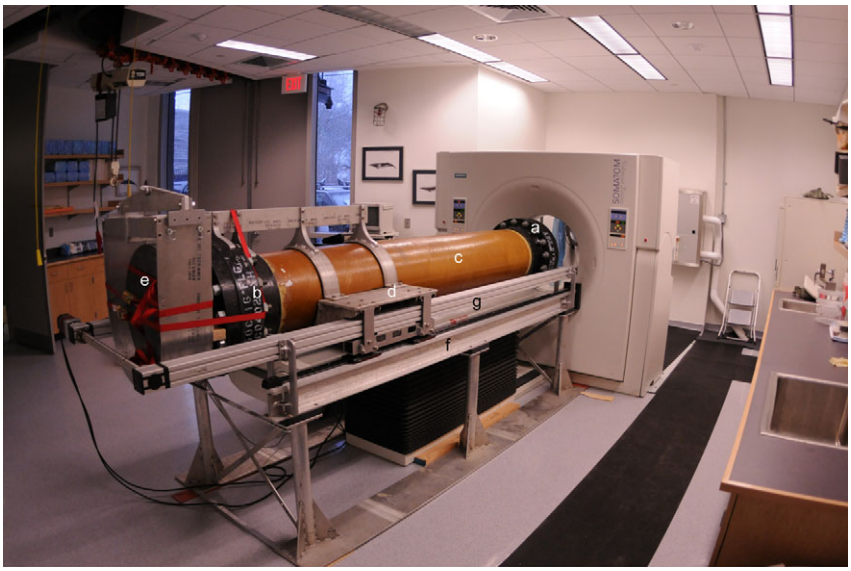

Fig. 1. Hyperbaric imaging system. The chamber consists of a fiberglass pipe with end flanges (a,b) and caps rated to 1720 kPa. A dead seal or dolphin is placed in the imaging portion (c), restrained with suction cups to the chamber wall, and the chamber filled with water. A hydraulic press allows pressurization to the desired depth equivalent. The chamber rests on a carriage (d) and it has a counterweight (e). The carriage runs on a pair of rails (f) to accommodate the loaded weight as that exceeds the scanner table capacity. The rails are motor driven *via* continuous belts (g) to follow the movement of the scanner table. Spiral CT scans were acquired for each subject at a series of pressures.

Triangle Park, NC, USA). The endotracheal tube was attached to a system of 3-way valves with a 3 l volumetric syringe (Series 5530, Hans-Rudolph Inc., Shawnee, KS, USA), which allowed inflation of the lungs at increments of 100 ml. After each experiment was concluded, gross necropsy and histological examinations were undertaken.

Specimen preparation

Specimens were first scanned in air using CT to ensure there was no evident lung pathology or pneumothorax. The specimens were then intubated by performing a ventral tracheotomy and attaching a ligature around the trachea and endotracheal tube to ensure administered air remained within the lungs, and water did not enter the trachea. A balloon catheter was inserted into the esophagus. The airway (P_{air}) and esophageal (P_{eso}) pressures were measured using differential pressure transducers (MPX type 339/2, Harvard Apparatus, Holliston, MA, USA) connected to an amplifier (Tam-A, Harvard Apparatus). The data were collected on a laptop using an A/D card (USB 1208LS, Measurement Computing, Norton, MA, USA) sampling at 2 Hz. The ambient pressure (P_{amb}) was used as a reference and set at 0 cm H_2O. We estimated total lung capacity (TLC) as the volume of air required to raise transpulmonary pressure (P_{tp}=P_{air}–P_{eso}) to 30 cm H_2O, a standard routinely used in lung physiology studies (Kooyman and Sinnett, 1982).

Following determination of TLC, the lungs were inflated initially to 100% and subsequently to 50% of TLC, and the valve on the endotracheal tube was then closed. To immobilize the specimen to avoid movement within the chamber when pressure changes altered specimen buoyancy, rubber suction cups (Part 8547A12, McMaster-Carr, Elmhurst, IL, USA) were attached to each appendage and the snout. The specimen was placed in sternal recumbency in the imaging portion of the chamber. The suction cups were then moistened with water and pressed manually onto the inner wall of the chamber. The end caps were attached to the chamber and the bolts tightened to 45 kg torque. Using a ceiling crane, the chamber was then filled with water *via* the lower nipple, with the chamber tilted up towards the imaging end by approximately 20 deg to bleed all remaining air *via* the upper nipple. Once there was a steady stream of water from the upper nipple, the upper valve was closed and the chamber was pressurized to the selected pressure. It was then lowered and secured to the rail bed, which spanned the scanner table.

CT scanner

A Siemens Somatom Volume Zoom 4-detector row multislice scanner (Siemens Medical Solutions USA Inc., Malvern, PA, USA) was used for all image acquisitions. All scans were performed using a high exposure helical scan protocol of 800 (effective) mA and 140 kV with a 0.5 s rotation time with 6 mm thick slices, using a 5 mm collimator and a table pitch of 10 mm. Two sets of reconstructions for each pressure were done at 6 mm intervals using B30 (soft tissue) and B70 (bone/lung) algorithms. Scans were made at each of three pressures (*circa* 1000, 520 and 0 kPa) at both 100% and 50% TLC inflations. To adjust the surface lung inflation, the system had to be removed from the scanner bed, the chamber drained, and the end cap removed to gain access to the endotracheal tube valve.

Scan analysis

Areas of each lung in each slice that included all lung tissue, but not the trachea and main stem bronchi, were manually selected using Osirix software (Pixmeo, Geneva, Switzerland, www.osirix-viewer.com). These segmentations allowed calculation of the total lung volume as the total sum of the product of each area and slice thickness. The mean Hounsfield units (HU) were measured within each lung area in each slice. To estimate the volume of gas in each slice of lung at each pressure, we used a previously published method (Patroniti et al., 2004) where the attenuation is assumed to represent a linear scale from –1000 HU (gas) to 0 HU (water equivalent attenuation tissues). In other words, a scan with attenuation of 0 HU would contain 100% water, whereas one with –1000 HU would be 100% gas, 0% tissue and/or fluid. We assumed that the lung was 100% compressed when the HU averaged zero. We then calculated the residual lung tissue volume at each pressure, as the difference between total lung and gas volume at each pressure. We plotted the resultant lung, lung gas and lung tissue volumes at 100% and 50% TLC for each of the four species. Lung compression was estimated by extrapolating the line from the middle and deep depths to where it intersected a volume of zero. Three-dimensional (3D) reconstructions of the lungs and estimates of tissue compartment volumes at each pressure were derived using Amira 5.2.2 software (Visage Imaging Inc., San Diego, CA, USA). Incisions associated with the tracheotomy limited our ability to reconstruct the head region.

Mean outside air temperature for the experimental period was –0.5°C; thus, the animals were naturally refrigerated during transport by sea and road before they entered the chiller prior to experimentation.

Gross necropsy and histopathology

After completion of the experimental series for each case, a gross necropsy was completed on each specimen. Major organs were examined for gross abnormalities and samples of each organ were placed in 10% buffered formalin, processed, sectioned at 5 µm, stained with hematoxylin and eosin, and examined by bright field microscopy for evidence of cellular disease. Specimens (Table 1) were evaluated for disease. D05952Pg showed acute pulmonary congestion and hemorrhage associated with drowning, and a localized area of eosinophilic arteritis in one section of lung, intestinal acanthocephalan parasites, and blunt trauma to the head, likely acquired during fishing gear entanglement at the time of death. D08883Hg was unremarkable grossly with the exception of some bruising at the occipital condyles. There was acute meningeal congestion and edema, acute pulmonary congestion, edema and atelectasis, acute mild myocardial necrosis, acute adrenal necrosis, all associated with drowning and peri-mortem trauma, and mild hepatitis. IFAW10-049Pp showed hepatic trematodiasis. The lungs

Table 1. Animals used for hyperbaric computed tomography

ID	Date of death (dd/mm/yy)	Species	Common name	Sex	Length (cm)	Mass (kg)	Source
D05952Pg	17.2.10	*Pagophilus groenlandicus*	Harp seal	F	99	27.5	Bycaught
D08883Hg	12.2.10	*Halichoerus grypus*	Gray seal	F	104	21.35	Bycaught
IFAW10-049Pp	22.2.10	*Phocoena phocoena*	Harbor porpoise	M	105	22.1	Single stranded
IFAW10-065Dd	27.2.10	*Delphinus delphis*	Short-beaked common dolphin	M	190	75.03	Mass stranded

Fig. 2. Computed tomography (CT) sections through the mid-thoracic region of the harbor porpoise at (A) 0, (B) 520 and (C) 1000 kPa (i.e. depth equivalents of 0, 50 and 100 m). The darker the tissue, the more gas it contains. The darkest quasi-circular structures are the bronchi, and these were excluded from the numerical volumes numerated in Fig. 4.

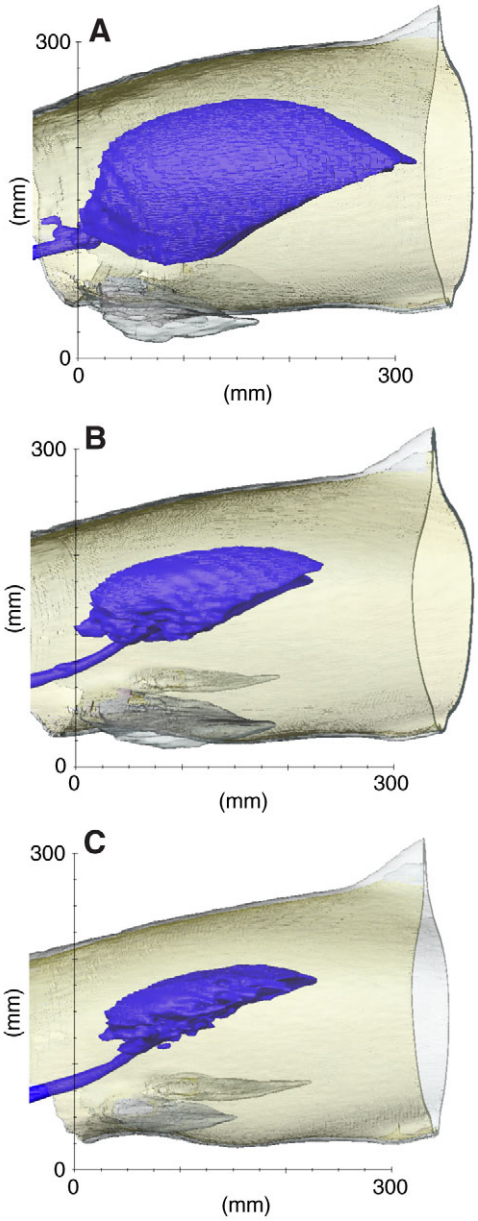

Fig. 3. Lateral view of three-dimensional reconstructions of the chest surface and lungs of the harbor porpoise at (A) 0, (B) 520 and (C) 1000 kPa (i.e. 0, 50 and 100 m depth equivalents). Note the obvious chest and lung compression with increasing depth.

were unremarkable. IFAW10-065Dd showed mild periportal hepatitis, mild multifocal histiocytosis, and interstitial pneumonia in both lungs, and pulmonary edema in the left lung, which was resistant to artificial inflation during the necropsy.

RESULTS

Information on specimens used in the experiments is listed in Table 1. The gross necropsy and histological examination that followed experimentation with each specimen confirmed that they were not significantly compromised by decomposition.

Initial trials with the chamber were undertaken without the animal being secured by suction cups. It became apparent that, as the pressure increased and the net buoyancy changed from positive to negative with lung compression, the specimen position changed from pressing against the top of the chamber to lying on the bottom of it. For the common dolphin, this change occurred between 0 and 50 m depth equivalent. It was also noted that, as the unrestrained animal twisted along the long axis of the body from the initial position of sternal recumbency, the lung that rested at the higher point in the chamber showed the least amount of attenuation (i.e. was least compressed). Suction cups were used to restrain specimens in subsequent experiments.

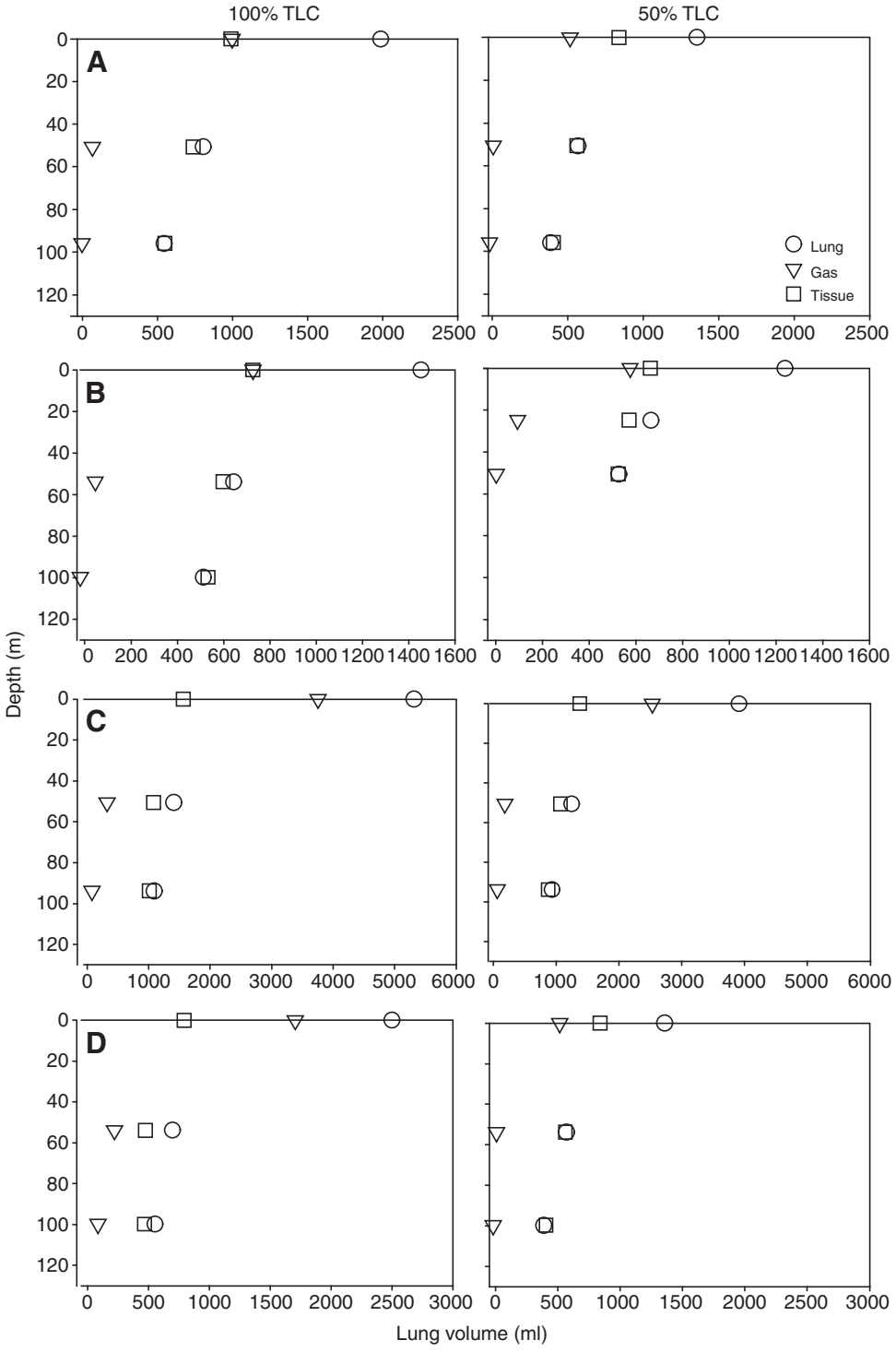

Fig. 4. Observed total lung volume, lung gas volume (calculated from CT attenuation as described in Materials and methods) and lung tissue volume (the difference between total lung and lung gas volumes) *versus* pressure for (A) harp seal, (B) gray seal, (C) common dolphin and (D) harbor porpoise. A valved endotracheal tube was inserted and then sealed after the lungs were inflated at surface pressure. The gas volume plots were extrapolated to a volume of zero to estimate the depth of lung compression shown in Table 2. Note the depth for 50% total lung capacity (TLC) for the gray seal was shallower than for the other experiments.

Fig. 2 shows transverse CT images (i.e. short-axis views across the body) of the mid-thoracic region of the harbor porpoise lungs at 0, 520 and 1000 kPa (0, 50 and 100 m depth equivalents) at an initial inflation of 100% TLC. With increasing pressure, the lung and chest wall were compressed but the dorsal portion of the lung remained inflated. Fig. 3 shows 3D models of the external surface of the harbor porpoise and lung surfaces at 0, 520 and 1000 kPa (0, 50 and 100 m depth equivalents). With increasing pressure, compression of the ventral portion of the chest wall was remarkable. Fig. 4 shows the total lung, lung tissue and lung gas volumes for the four specimens at the three pressures (i.e. 0, 50 and 100 m depth equivalents) at lung inflations of 100% and 50% TLC. The estimated depth of lung compression for each species, derived from Fig. 4 (as described in Materials and methods), is shown in Table 2. Measurements of the various tissue volumes in the harbor porpoise are shown in Table 3. With increasing pressure, lung volume decreased, while the volumes of the non-gas-containing tissues did not change significantly. Note that the lung volume measured in Table 3 for the porpoise includes lung tissue and gas, hence the greater total lung volume than the measured TLC shown in Table 2.

Table 2. Estimated depth of compression of lungs inflated to 100% or 50% TLC at the surface for four marine mammal species

Species	TLC (ml)	100% TLC compression depth (m)	50% TLC compression depth (m)
Harp Seal	1200	94	59
Gray seal	1200	93	58
Harbor porpoise	1800	133	84
Common dolphin	3000	115	118

Lung compression was defined by a mean attenuation of 0 HU in lung tissue (see Materials and methods).
TLC, total lung capacity.

DISCUSSION

Much of our understanding of the diving physiology and resistance to DCS of marine mammals is based on a careful assessment of the depth at which lung atelectasis induces a 100% pulmonary shunt. Indirect measurements have suggested that the depth where gas exchange ceases is between 30 m (Falke et al., 1985) and 70 m (Ridgway and Howard, 1979), but direct measurements of animals diving with a lung volume of only 18% of TLC indicate that complete shunt may not occur until a depth of 170 m (Kooyman and Sinnett, 1982). Studies of maximal depth of neutral buoyancy, which has to be at a depth less than atelectasis (Biuw et al., 2003; Skrovan et al., 1999; Williams et al., 2000), agree with the pulmonary shunt data published by Kooyman and Sinnett showing that the collapse occurs at depths below 100 m (Kooyman and Sinnett, 1982). Our results using the hyperbaric chamber suggest these last estimates have worth. Lung compression occurs differentially according to position within the body (Fig. 2) and at much greater depths than previously thought (see Tables 2 and 3). These findings require that we reopen the discussion as to whether marine mammals are susceptible to DCS. The data we present here add credence to findings and hypotheses on the subject of susceptibility to and manifestation of DCS in bycaught and stranded marine mammals (Fernandez et al., 2005; Jepson et al., 2005; Moore et al., 2009). The data add further weight to the suggestion that marine mammals may experience supersaturation at levels that may result in asymptomatic or symptomatic inert gas bubbles when diving repetitively, acquired when lung collapse is incomplete (Hooker et al., 2009). Exposure to irritating levels of sonar could alter and hence stress dive patterns and enhance the risk of DCS by affecting the ability to behaviorally manage saturation levels. Reassessment of dive patterns in conjunction with these findings may provide better understanding of the behavior and physiology of different species. Future studies using live animals are necessary in order to determine how relevant these post-mortem experiments are to live animals and whether physiological changes to circulation influence the depth at which the lungs fully compress.

The CT images show a gradually increasing attenuation of the lung with pressure as air in the lungs and airways is compressed and chest volume decreases (Figs 2 and 3 and Tables 2 and 3). In Fig. 4 we show changes in lung volume from three perspectives: total lung volume (excluding trachea and bronchi), lung gas and lung tissue (the cells and fluids that along with gas form the full lung volume). The lung tissue volumes show a slight and quite linear reduction with pressure. This is because we are inevitably including the bronchioles in this measurement segment, which appear to be still compressing with pressure. The major change in total lung volume parallels the reduction in gas volume.

Table 3. Volume (ml) of anatomical structures of a harbor porpoise at different depths (0, 50, 100 m) with lungs inflated to 100% TLC

Structure	0 m	50 m	100 m
Skin	1425	1320	1305
Lung	2775	757	438
Blubber	4369	4407	4430
Bone	1158	1158	1263
Brain/spinal cord	451	458	441
Cranial air	33	6	11
Other tissues	5724	6254	6345

TLC, total lung capacity

The least amount of lung attenuation was observed in the highest portion of lung within the chamber, bilaterally when animals were restrained in sternal recumbency by suction cups, and unilaterally in the animal that was free to twist under pressure. This suggests that the very small but finite pressure difference within the chamber, driven by the difference in height, was sufficient to initiate lung compression in the lowest sections of the lungs, which then spread to the higher sections as pressure increased (clear gradient in Fig. 2). Thus, we would predict that diving mammals that deviate from a dorsal-up position would have differentially compressed lungs depending on body orientation. Any asymmetry in lung compression would in turn affect net regional buoyancy and might have consequences for swimming/foraging effort. In essence, animals that are headed downwards would likely have less lung compression in the caudal lung poles, and in the cranial lung poles on ascent. It would be worth examining the anatomy of diving vertebrate lungs to look for structural corollaries to this prediction.

In contrast to the other three species examined, the estimated depth of lung compression for the 50% TLC common dolphin lungs shown in Table 2 exceeded that of the lungs inflated to 100% TLC. The explanation for this is that the histological pneumonia and resistance to inflation during necropsy described in the common dolphin specimen may well have changed the 100% TLC lung behavior under increasing pressure. The other specimens had essentially normal lungs, albeit with some changes associated with drowning in the harp and gray seals. We did consider discarding the experimental data from the common dolphin but, given that varying degrees of gross and histological lung change are commonly found in wild dolphins and seals, we decided to report our findings as they provide a window into the pathophysiology of how these animals live despite various disease states. These conditions are often associated with bacteria and parasites. It is unclear whether these infections are the primary agents, or at times secondary to repeated mild trauma associated with endless cycles of lung compression and re-inflation with each dive. Irrespective of which comes first, the combination of trauma potential and infectious agents must impact dive endurance if changes such as we show here in terms of lung compression behavior are commonly associated with unhealthy lungs. It is significant that in a broad survey of causes of mortality of stranded marine mammals in the Cape Cod (MA, USA) area (Bogomolni et al., 2010), disease was the commonest cause of death, and bacterial pneumonia was a major contributor to this. Thus, variation in lung compression depth will be caused by diving behavior and health.

There are a number of other factors that may impact our findings: post-mortem autolysis and decomposition, the lack of blood flow, the difference between lung compression and alveolar collapse, and the use of a rigid endotracheal tube impairing the compliance of the upper airway. Although post-mortem decomposition (autolysis and bloating) is a major concern with any experiment on a dead animal, neither was observed grossly or histologically. Fortunately, our major seasonal windows of access to both stranded and bycaught marine mammal specimens in New England is the period between November and March. Transport of specimens at the seasonally low ambient temperatures does not induce rapid decomposition. Although our post-mortem specimens had no cardiovascular or interstitial fluid and lymph movement, and no vasomotor, blood gas, pH, core temperature or peripheral temperature control, nor other processes that the brain monitors during a routine dive, these experiments approximate the passive physical biomechanical envelope of a marine mammal body interacting with the pressures associated with diving to specific depths. They provide the physical baseline upon which live animal data can be layered by other studies. Live animal experiments in this system are certainly conceivable but bring with them a host of ethical and practical concerns. They are, however, an essential next step in these studies. A further limitation of our experimental system was the presence of a semi-rigid endotracheal tube, controlling the addition of measured volumes of air at surface pressure, and *via* the valve system allowing retention of this gas during pressurization. It did, however, impact the compliance and hence biomechanical response of the cranial air spaces and upper trachea, influencing the behavior of the lung. Bostrom and colleagues have discussed the role of tracheal flexibility in determining the depth of alveolar collapse (Bostrom et al., 2008). Thus, an improvement for our system would be to develop a valved rubber cup closure for the mouth and nares (nostril or blowhole). However, the flexibility of this portion of the respiratory tract (M.J.M. and A.F., unpublished observations) suggests upper airway compression would have resulted in even deeper depths of lung compression (Bostrom et al., 2008) were this to have been incorporated.

Our goal was to use the principle of this technique to test the basic assumption that passive lung compression occurs in a graded and predictable fashion as indicated by previous studies (Kooyman and Sinnett, 1982). Despite the paucity of samples that we report (caused by prohibitive time and labor costs associated with these measurements), we showed that lung compression depth may be greater than previously thought by some. Compression depths appear to be greater for cetaceans than for pinnipeds (Table 2) even when both are given full initial lung capacities. Many phocid seals exhale prior to diving (Scholander, 1940), which would increase this difference further, although others, such as Weddell seals, dive with some residual volume (Kooyman et al., 1971). Our findings do not suggest a body mass effect as the examined porpoise had a comparable body mass to the seals (Table 1) but a deeper depth of lung compression. Subjectively, post-mortem dolphins and porpoises appear to have a stiffer chest than pinnipeds, although the more horizontal orientation of the odontocete diaphragm, compared with that of the pinniped, might compensate for this by enabling greater abdominal compression of the thoracic contents. Whether these are purely post-mortem-dependent differences remains to be determined in studies on live animals, but this observation concurs with previous inference about chest compliance differences between seals and cetaceans from live seals (Falke et al., 1985) and dolphins (Ridgway and Howard, 1979).

Modeling of lung collapse in human breath-hold divers suggests that it occurs at the much greater depth of 235 m (Fitz-Clarke, 2007). It would be instructive to undertake a study of a terrestrial mammalian specimen such as a pig and use the experimental system described here. Importantly, Fitz-Clarke emphasizes that ‘collapse depth cannot be determined by simply applying Boyle’s law to the volume of the alveoli at ambient pressure because the stiffer embedded conducting airways account for a progressively greater relative volume contribution as lungs approach the degassed state’ (Fitz-Clarke, 2007). It is also important to realize that gross observation of lung compression does not necessarily predict the depth of functional alveolar collapse, where there is no longer gas in close proximity to the alveolar capillaries, which is the depth at which blood and tissue gas partial pressures can no longer increase through ready diffusion. Higher resolution CT scans using our system may permit better observation of lung parenchyma under pressure. Measurement of the depth of pulmonary shunt concurs with our findings that lung compression is deeper than previously estimated by some: Kooyman and Sinnett show that for a harbor seal diving with a lung volume that is only 18%, the shunt is about 65–80% at 90 m and they extrapolate that collapse probably occurs somewhere close to 170 m (Kooyman and Sinnett, 1982).

Future developments of the model described in this study include a hyperbaric chamber with a functional magnetic resonance imaging system. This system would require the hyperbaric chamber and other materials within the scanner to be constructed from non-magnetic materials. The use of polarized gas would further enhance lung imaging. It is also possible to conceive of using live animals within a CT hyperbaric system. Modifications would have to include a more efficient mechanism to both open and close the chamber, and to fill and empty it with water. Suitably trained animals would also be required. To introduce exercise associated with normal diving behavior, it is perhaps possible to conceive a self-contained flume system, with an integral pump to create a controlled water flow past the subject. Smaller subjects would substantially ease the logistics. Thus, this concept is perhaps best first attempted in a turtle.

In conclusion, we have for the first time combined pressure with imaging *via* a CT scanner interfaced to a hyperbaric chamber, and investigated the interaction of pressure with the biomechanics of diving mammals such as seals and dolphins. This allowed us to generate valuable observations on the progressive compression of diving mammal lungs at depths greater than previously reported by some.

ACKNOWLEDGEMENTS

Funding for this work was provided by the US Office of Naval Research Award Number: N000140811220. We are grateful to the Northeast Fisheries Observer Program, Betty Lentell and William Greer, the International Fund for Animal Welfare Marine Mammal Rescue and Research Division, and Katie Touhey and Misty Niemeyer for the experimental subjects, the demise of which was unrelated to this study. We thank Darlene Ketten for her advice. Greg Early and Crill Carlson assisted with necropsies. Michael Garner and David Rotstein undertook the histopathology. Massimo Ferrigno kindly loaned equipment. Sascha Hooker and two anonymous reviewers significantly improved the manuscript.

REFERENCES

Biuw, M., McConnell, B., Bradshaw, C. J. A., Burton, H. and Fedak, M. (2003). Blubber and buoyancy: monitoring the body condition of free-ranging seals using simple dive characteristics. *J. Exp. Biol.* **206**, 3405-3423.

Bogomolni, A. L., Pugliares, K. R., Patchett, K., Herzig, S. M., Harry, C. T., LaRocque, J. M., Touhey, K. M. and Moore, M. J. (2010). Mortality trends of stranded marine mammals on Cape Cod and Southeastern Massachusetts between 2000-2006. *Dis. Aquat. Org.* **88**, 143-155.

Bostrom, B. L., Fahlman, A. and Jones, D. R. (2008). Tracheal compression delays alveolar collapse during deep diving in marine mammals.. *Respir. Physiol. Neurobiol.* **161**, 298-305.

Costa, D. P., Kuhn, C. E., Weise, M. J., Shaffer, S. A. and Arnould, J. P. Y. (2004). When does physiology limit the foraging behaviour of freely diving mammals? *Int. Congr. Ser.* **1275**, 359-366.

Cox, T. M., Ragen, T. J., Read, A. J., Vos, E., Baird, R. W., Balcomb, K., Barlow, J., Caldwell, J., Cranford, T., Crum, L. et al. (2006). Understanding the impacts of anthropogenic sound on beaked whales. *J. Cetacean Res. Manag.* **7**, 177-187.
Data, P., Montemaggiori, L., Motamed, A. and Di Leo, V. (1979). Thoracic and pulmonary radiographic modification during immersion in apnea: 1 – a special apparatus. *Boll. Soc. Ital. Biol. Sper.* **55**, 24-26.
Falke, K. J., Hill, R. D., Qvist, J., Schneider, R. C., Guppy, M., Liggins, G. C., Hochachka, P. W., Elliott, R. E. and Zapol, W. M. (1985). Seal lungs collapse during free diving: evidence from arterial nitrogen tensions. *Science* **229**, 556-557.
Fernandez, A., Edwards, J. F., Rodriguez, F., Espinosa De Los Monteros, A., Herraez, P., Castro, P., Jaber, J. R., Martin, V. and Arbelo, M. (2005). Gas and fat embolic syndrome involving a mass stranding of beaked whales (Family *Ziphiidae*) exposed to anthropogenic sonar signals. *Vet. Pathol.* **42**, 446-457.
Fish, F. E. (1996). Transitions from drag-based to lift-based propulsion in mammalian swimming. *Am. Zool.* **36**, 628-641.
Fitz-Clarke, J. R. (2007). Mechanics of airway and alveolar collapse in human breath-hold diving. *Respir. Physiol. Neurobiol.* **159**, 202-210.
Fossette, S., Gleiss, A. C., Myers, A. E., Garner, S., Liebsch, N., Whitney, N. M., Hays, G. C., Wilson, R. P. and Lutcavage, M. E. (2010). Behaviour and buoyancy regulation in the deepest-diving reptile: the leatherback turtle. *J. Exp. Biol.* **213**, 4074-4083.
Harrison, R. J. and Tomlinson, J. D. W. (1960). Normal and experimental diving in the common seal (*Phoca vitulina*). *Mammalia* **24**, 386-399.
Hays, G., Metcalfe, J. and Walne, A. (2004). The implications of lung-regulated buoyancy control for dive depth and duration. *Ecology* **85**, 1137-1145.
Hooker, S. K., Baird, R. W. and Fahlman, A. (2009). Could beaked whales get the bends? Effect of diving behaviour and physiology on modelled gas exchange for three species: *Ziphius cavirostris*, *Mesoplodon densirostris* and *Hyperoodon ampullatus*. *Respir. Physiol. Neurobiol.* **167**, 235-246.
Jepson, P. D., Arbelo, M., Deaville, R., Patterson, I. A. P., Castro, P., Baker, J. R., Degollada, E., Ross, H. M., Herráez, P., Pocknell, A. M. et al. (2003). Gas-bubble lesions in stranded cetaceans. *Nature* **425**, 575.
Jepson, P. D., Deaville, R., Patterson, I. A. P., Pocknell, A. M., Ross, A. M., Baker, F. E., Howie, J. R., Reid, R. J., Colloff, A. and Cunningham, A. A. (2005). Acute and chronic gas bubble lesions in cetaceans stranded in the United Kingdom. *Vet. Pathol.* **42**, 291-305.
Kooyman, G. L. (1985). Physiology without restraint in diving mammals. *Mar. Mamm. Sci.* **1**, 166-178.
Kooyman, G. L. (2006). Mysteries of adaptation to hypoxia and pressure in marine mammals. *Mar. Mamm. Sci.* **22**, 507-526.
Kooyman, G. L. and Sinnett, E. E. (1982). Pulmonary shunts in harbor seals and sea lions during simulated dives to depth. *Physiol. Zool.* **55**, 105-111.
Kooyman, G. L., Hammond, D. D. and Schroeder, J. P. (1970). Bronchograms and tracheograms of seals under pressure. *Science* **169**, 82-84.
Kooyman, G. L., Kerem, D. H., Campbell, W. B. and Wright, J. J. (1971). Pulmonary function in freely diving Weddell seals, *Leptonychotes weddelli*. *Respir. Physiol.* **12**, 271-282.
Miller, P. J. O., Johnson, M. P., Tyack, P. L. and Terray, E. A. (2004). Swimming gaits, passive drag and buoyancy of diving sperm whales *Physeter macrocephalus*. *J. Exp. Biol.* **207**, 1953-1967.
Moore, M. J. and Early, G. (2004). Cumulative sperm whale bone damage and the bends. *Science* **306**, 2215.
Moore, M. J., Bogomolni, A. L., Dennison, S. E., Early, G., Garner, M. M., Hayward, B. A., Lentell, B. J. and Rotstein, D. S. (2009). Gas bubbles in seals, dolphins and porpoises entangled and drowned at depth in gill nets. *Vet. Pathol.* **46**, 536-547.
Nowacek, D. P., Johnson, M. P., Tyack, P. L., Shorter, K., McLellan, W. A. and Pabst, D. A. (2001). Buoyant balaenids: the ups and downs of buoyancy in right whales. *Proc. R. Soc. Lond. B* **268**, 1811-1816.
Patroniti, N., Bellani, G., Manfio, A., Maggioni, E., Giuffrida, A., Foti, G. and Pesenti, A. (2004). Lung volume in mechanically ventilated patients: measurement by simplified helium dilution compared to quantitative CT scan. *Intensive Care Med.* **30**, 282-289.
Paulev, P. (1965). Decompression sickness following repeated breath-hold dives. *J. Appl. Physiol.* **20**, 1028-1031.
Ridgway, S. H. and Howard, R. (1979). Dolphin lung collapse and intramuscular circulation during free diving: evidence from nitrogen washout. *Science* **206**, 1182-1183.
Scholander, P. F. (1940). Experimental investigations on the respiratory function in diving mammals and birds. *Hvalradets Skrifter* **22**, 1-131.
Skrovan, R. C., Williams, T. M., Berry, P. S., Moore, P. W. and Davis, R. W. (1999). The diving physiology of bottlenose dolphins (*Tursiops truncatus*)-II. Biomechanics and changes in buoyancy at depth. *J. Exp. Biol.* **202**, 2749-2761.
Watanabe, Y., Baranov, E. A., Sato, K., Naito, Y. and Miyazaki, N. (2006). Body density affects stroke patterns in Baikal seals. *J. Exp. Biol.* **209**, 3269-3280.
Williams, T. M., Davis, R. W., Fuiman, L. A., Francis, J., Le Boeuf, B. J., Boeuf Horning, M., Calambokidis, J. and Croll, D. A. (2000). Sink or swim: strategies for cost-efficient diving by marine mammals. *Science* **288**, 133-136.
Wilson, R., Hustler, K., Ryan, P., Burger, A. E. and Noldeke, E. C. (1992). Diving birds in cold water: do Archimedes and Boyle determine energetic costs? *Am. Nat.* **140**, 179-200.
Zimmer, W. and Tyack, P. (2007). Repetitive shallow dives pose decompression risk in deep-diving beaked whales. *Mar. Mamm. Sci.* **23**, 888-925.